

Extending the rotational spectrum of cyclopentadiene towards higher frequencies and vibrational states

Luis Bonah^a, Benedikt Helmstaedter^a, Jean-Claude Guillemin^b, Stephan Schlemmer^a, Sven Thorwirth^a

^a*I. Physikalisches Institut, Universität zu Köln, Zùlpicher Str. 77, Köln, 50937, Germany*

^b*Univ Rennes, Ecole Nationale Supérieure de Chimie de Rennes, ISCR-UMR 6226, Rennes, 35000, France*

Abstract

Cyclopentadiene ($c\text{-C}_5\text{H}_6$) is a cyclic pure hydrocarbon that was already detected astronomically towards the prototypical dark cloud TMC-1 (Cernicharo et al. 2021, *Astron. Astrophys.* **649**, L15). However, accurate predictions of its rotational spectrum are still limited to the microwave region and narrow quantum number ranges. In the present study, the pure rotational spectrum of cyclopentadiene was measured in the frequency ranges 170–250 GHz and 340–510 GHz to improve the number of ground vibrational state assignments by more than a factor of 20, resulting in more accurate rotational parameters and the determination of higher-order centrifugal distortion parameters. Additionally, vibrational satellite spectra of cyclopentadiene in its eight energetically lowest vibrationally excited states were analyzed for the first time. Coriolis interactions between selected vibrational states were identified and treated successfully in combined fits. Previous microwave work on the three singly ^{13}C substituted isotopologues was extended significantly also covering frequency ranges up to 250 GHz. The new data sets permit reliable frequency predictions for the isotopologues and vibrational satellite spectra far into the sub-mm-wave range. Finally, the experimental rotational constants of all available isotopologues and calculated zero-point vibrational contributions to the rotational constants were used to derive a semi-experimental equilibrium structure of this fundamental ring molecule.

Keywords: rotational spectroscopy, vibrationally excited states, Coriolis interaction, absorption spectroscopy

1. Introduction

Cyclopentadiene ($c\text{-C}_5\text{H}_6$) is a polar cyclic hydrocarbon with an appreciable dipole moment of 0.419(4) D [1]. In the laboratory, its rotational spectrum was first studied in the microwave by Laurie in 1956 [2]. Later studies measured more microwave transitions [1, 3] and extended the frequency coverage into the mm-wave region up to 390 GHz [4]. However, even in the most recent work by Bogey et al. [4] only 99 lines were reported. The resulting parameters have high uncertainties and no sextic or higher-order parameters were fitted. Therefore, the accuracy for predictions outside the measured frequency and quantum number range leaves much room for improvement. In addition to the main isotopologue, the three singly ^{13}C substituted isotopologues and different deuterium-substituted isotopologues were examined [1, 5] in the microwave

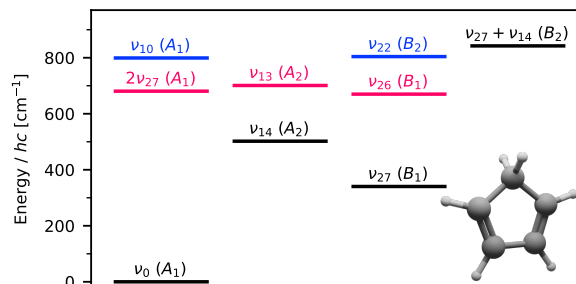


Figure 1: The vibrational states of cyclopentadiene below 850 cm^{-1} . The respective symmetries are given in parentheses. The two interaction systems are indicated by blue and red color.

regime, but no mm-wave data are available. No vibrational satellite spectra have been reported so far for any isotopic species and only one vibrational band has been studied at high spectral resolution,

the ν_{26} fundamental mode of the parent isotopologue [6]. However, eight vibrational states lie below 850 cm^{-1} with the methylene-rocking motion being the lowest at about 350 cm^{-1} (see Fig. 1) [7]. The narrow spacing between some vibrational levels suggests they might be subject to considerable interactions.

Cyclopentadiene was detected astronomically towards TMC-1 [8] via five lines with low quantum numbers ($2 \leq J \leq 5$ and $K_a \leq 3$) around 38 GHz and 46 GHz, all of which belong to the ground vibrational state of the main isotopologue.

This work aims at extending the frequency and quantum number coverage of the main isotopologue and the singly ^{13}C substituted isotopologues. Additionally, for the parent isotopic species, rotational analyses of all vibrationally excited states below 850 cm^{-1} are presented, including a treatment of two resonance systems identified for the first time.

2. Experimental details

High-resolution broadband spectra of cyclopentadiene were recorded with an absorption spectrometer in the frequency ranges 170–250 GHz and 340–510 GHz. A commercially available radiation source from Virginia Diodes was combined with two different amplifier-multiplier chains to reach the desired frequency ranges. A 5 m absorption cell was used in a double-pass setup for a total absorption path of 10 m. On the detection side, a Schottky detector was employed with subsequent preamplifiers and a lock-in amplifier. The radio frequency was frequency modulated by the synthesizer and a $2f$ demodulation of the detector signal was performed by the lock-in amplifier to increase the signal-to-noise ratio (SNR). The resulting lineshapes look similar to a second derivative Voigt profile. The spectrometer was described in greater detail elsewhere previously [9].

Commercially, cyclopentadiene is not available in monomeric form but as a Diels-Alder adduct, dicyclopentadiene. It may however be produced from the adduct through a thermally induced retro-Diels-Alder reaction. In the present study, the thermolysis used a quartz tube, an oven with a 10 cm heating zone and a temperature of about 560°C which was determined to yield optimal production for this specific setup [10]. A needle valve attached to the sample container allowed to precisely set the precursor flow. To increase the vapor pressure of dicyclopentadiene and prevent clogging of the needle valve,

the sample container and the valve were resistively heated to about 55°C . The rotational temperature in the absorption cell was room temperature as is apparent from the rotational spectrum (see e.g. the good agreement between the experimental intensities and the predictions performed at 300 K in Fig. 2). Due to the thermolysis, all measurements were performed under mild flow conditions while keeping the pressure in the cell in the range of 20–30 μbar . Standing waves were removed from the raw spectral data via Fourier filtering with a self-written script¹.

3. Spectroscopic fingerprint of cyclopentadiene

Cyclopentadiene is an asymmetric top rotor close to the oblate limit as seen from its Ray’s asymmetry parameter $\kappa = (2B - A - C)/(A - C) = 0.90$. The main isotopologue has C_{2v} symmetry² resulting in the two spin species ortho ($K_a + K_c$ odd) and para ($K_a + K_c$ even) with statistical weights of 9 and 7, respectively [6, 8]. Only the b -type dipole moment is non-zero (0.419(4) D [1]) and the rotational spectrum mainly comprises two characteristic patterns for $\Delta J = 1$ (R -branch) and $\Delta J = 0$ (Q -branch) transitions which are highlighted in Fig. 2.

The R -branch line series consist of $\Delta J_{\Delta K_a, \Delta K_c} = 1_{\pm 1, 1}$ transitions. For high J values the $\Delta K_a = +1$ transitions are blended with the respective $\Delta K_a = -1$ transitions. Transitions with the same $J + K_a$ value form patterns (see red lines in Fig. 2) that increase in J with increasing frequency. When K_a is far from J , the lines are spaced almost equidistantly (about 430 MHz). These patterns repeat every 8.54 GHz corresponding to $2(B + C - A) = 2C$ for the limiting case of an oblate symmetric top.

Q -branches comprise $\Delta J_{\Delta K_a, \Delta K_c} = 0_{1, -1}$ transitions and again the two asymmetry components are typically blended. Lines belonging to a single pattern (see blue lines in Fig. 2) share the same K_c value. Going from high to low frequencies, the pattern starts with the $K_a'' = 0$ transition and its respective blended $K_a'' = 1$ transition. Subsequent lines (at lower frequencies) increase in J and K_a . Similarly, the distance between lines increases

¹<https://github.com/Ltotheois/SnippetsForSpectroscopy/tree/main/FFTCorrection>

²The naming of the symmetry species B_1 and B_2 is swapped in this work compared to some older works, e.g. Castellucci et al. [7].

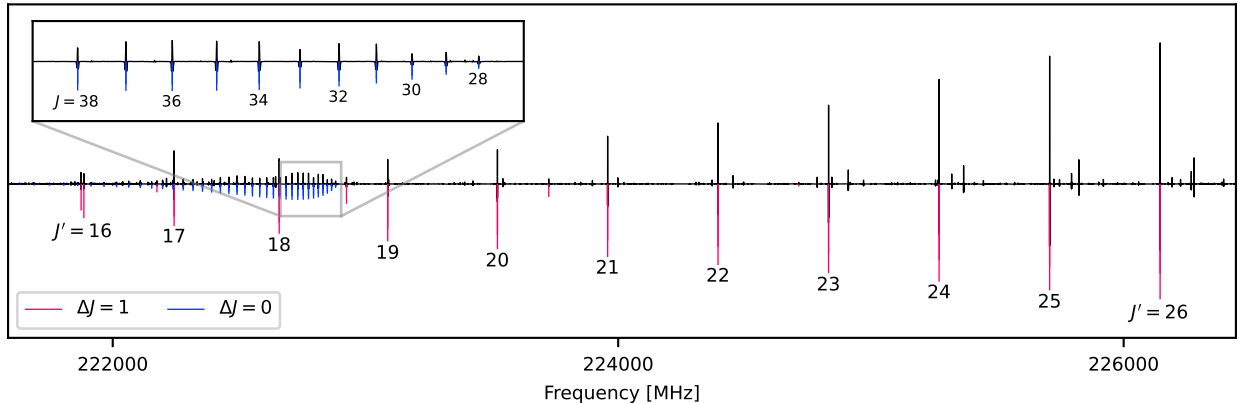


Figure 2: Part of the experimental spectrum of cyclopentadiene in black. Typical $\Delta J = 1$ and $\Delta J = 0$ patterns of the b -type spectrum of cyclopentadiene are highlighted by the corresponding predictions in red and blue, respectively. The R -branch transitions are governed by $\Delta J_{\Delta K_a, \Delta K_c} = 1_{\pm 1, 1}$ with $K'_a = 26 - J'$ or $27 - J'$ and J' as indicated. In the zoom-in, Q -branch transitions obey $\Delta J_{\Delta K_a, \Delta K_c} = 0_{1, -1}$ and $K'_a = J - 27$ or $J - 26$.

Table 1: The resulting rotational parameters for the ground vibrational states of the main isotopologue and the three singly ^{13}C substituted isotopologues.

Parameter	$c\text{-C}_5\text{H}_6$	$1\text{-}^{13}\text{C}$	$2\text{-}^{13}\text{C}$	$3\text{-}^{13}\text{C}$
A	/MHz 8426.108 825(35)	8226.0534(18)	8420.043 51(98)	8345.133 00(94)
B	/MHz 8225.640 352(33)	8219.4832(18)	8040.4326(14)	8108.7105(12)
C	/MHz 4271.437 296(30)	4217.759 07(40)	4219.409 81(37)	4219.064 93(33)
$-D_J$	/kHz -2.692 726(21)	-2.6502(22)	-2.6318(19)	-2.6357(17)
$-D_{JK}$	/kHz 4.059 634(34)	3.9985(49)	3.9703(41)	3.9771(38)
$-D_K$	/kHz -1.682 765(22)	-1.6585(26)	-1.6472(22)	-1.6498(21)
d_1	/Hz -42.220(10)	a	-17.2(13)	-12.7(13)
d_2	/Hz -0.6014(36)	a	-5.06(60)	1.90(51)
H_J	/mHz 1.0208(37)	a	a	a
H_{JK}	/mHz -4.0297(71)	a	a	a
H_{KJ}	/mHz 5.0425(73)	a	a	a
H_K	/mHz -2.0316(41)	a	a	a
Transitions	3510	228	228	235
Lines	1992	120	143	145
RMS	/kHz 21.40	14.97	16.72	16.31
$WRMS$	0.79	0.44	0.49	0.46

Fits performed with SPFIT in the S-reduction and III¹ representation. Standard errors are given in parentheses. Parameters of the ground vibrational state are applied to all vibrationally excited states and difference values are fitted. ^a Parameter was fixed to the global value.

slightly when J values increase. These Q -type patterns repeat about every 8.1 GHz, which for the limiting case of an oblate symmetric top would be given by $2(2B - A - C) = 2(B - C)$.

Spectroscopic assignment was carried out via Loomis-Wood plots as implemented in the LLWP software [11]. Pickett's SPFIT was used for least squares fitting to an asymmetric top Hamiltonian in the S-reduction and III¹ representation [12]. Line uncertainties were determined with a semi-automatic procedure described previously [13].

Complementary quantum chemical calculations in support of the spectroscopic analysis were performed using the CFOUR suite of programs [14, 15] using strategies outlined elsewhere [16]. Most im-

portantly, the rotation-vibration interaction constants $\alpha_i^{A,B,C}$ as well as vibrational wavenumbers $\tilde{\nu}_i$ were derived from an anharmonic force field computed at the coupled-cluster (CC) singles and doubles level extended by a perturbative correction for the contribution from triple excitations, CCSD(T), [17] in combination with the ANO0 basis set [18] and in the frozen core (fc) approximation. A high-level equilibrium structure of cyclopentadiene was calculated at the CCSD(T)/cc-pwCVQZ level (cf. Ref [19] and references therein) considering all electrons (ae) in the correlation treatment.

Assigning the spectrum of the main isotopologue was straightforward due to literature data covering frequencies up to 390 GHz [4] and readily visible patterns. Literature data from frequency ranges not covered here [1, 3, 4] were incorporated into our analysis except data from Laurie [2] as their data shows a systematic offset (mean $\nu_{\text{obs}} - \nu_{\text{calc}}$ value of 136(114) kHz) and because most of their lines were remeasured in later works.

Substituting a single ^{12}C with a ^{13}C atom has considerable influence on the observed spectrum. When substituting the 1-C atom³, the a - and b -axes are swapped. Therefore, the A constant of the $1\text{-}^{13}\text{C}$ isotopologue should be compared with the B constants of the other isotopologues and an a -type spectrum is observed. Substituting the 2-C or 3-C atom lifts the C_{2v} symmetry and rotates the prin-

³The labeling of carbon atoms is equivalent to the one in Scharpen et al. [1], where 1-C is the methylene carbon atom and the other carbons are numbered sequentially.

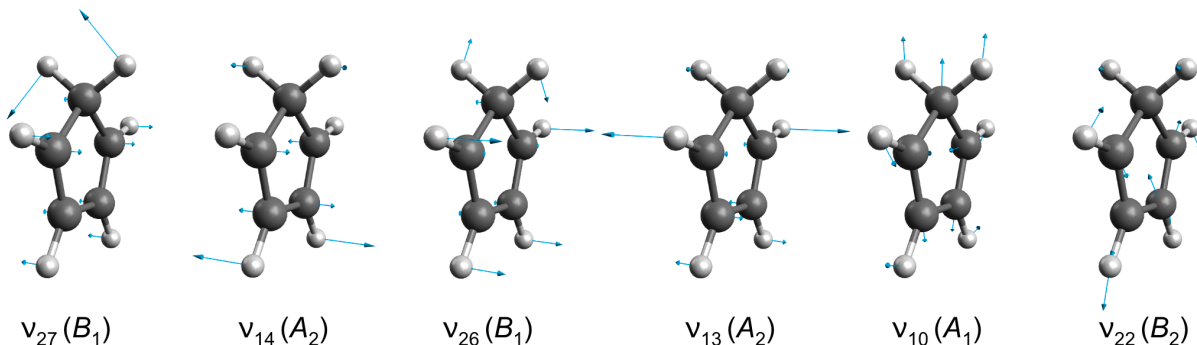


Figure 3: The six energetically lowest vibrational fundamentals sorted to increasing energy from left to right.

principal axes in the $a - b$ plane introducing an a -type dipole moment with a ratio μ_a/μ_b of 0.12 and 0.50, respectively [1]. Literature data covering lower frequencies were included in the analyses presented here [1]. Due to the low natural abundance, the analysis of the singly ^{13}C substituted isotopologues was limited by their low SNR to frequencies below 250 GHz.

The resulting parameters for the ground vibrational states of the isotopologues (see Tab. 1) show good agreement with literature data (see Tab. B.2⁴), although generally not within quoted uncertainties. As no literature data were available for the quartic centrifugal distortion constants of the singly substituted ^{13}C isotopologues, these values were derived (for all analyzed isotopologues) from fc-CCSD(T)/ANO0 force field calculations (see Tab. B.3). The good agreement between the calculated and experimental values confirms the physical meaningfulness of the experimental parameters with the exception of the d_2 parameter of the parent isotopic species. This deviation might be a consequence of the very small magnitude of this parameter for the parent species combined with the influence of zero-point vibration. Trial fits of the parent isotopic species using the I^Γ representation reveal proper agreement between the experimental and calculated quartic centrifugal distortion constants at the cost of an overall degraded fit quality. The new global fits are extended significantly regarding the number of assigned transitions as well as the frequency and quantum number coverage. Compared to previous results, additional higher-

order parameters were added and the accuracy of existing parameters was improved.

Vibrational motions of the six energetically lowest vibrational fundamentals are shown in Fig. 3. While the calculated vibrational wavenumbers show good agreement with literature values [7], there are substantial deviations of opposite sign for the α_i^C values of the ν_{10} and ν_{22} fundamentals. The magnitude combined with the mirror-like appearance of the deviations suggests that they result from contributions of Coriolis coupling to the rotational constants [20–22]. As a result, the search for the vibrational states ν_{10} and ν_{22} did not rely on calculated predictions but on finding their spectroscopic patterns by visual means alone, a task challenged by the diminished intensity of the vibrational satellites due to their small Boltzmann factors of only 2%. To support the identification of low-intensity patterns, already assigned states were removed from the spectrum by deleting the experimental data points around their peak position. This was done in an iterative process for the strongest remaining pattern(s) as shown in Fig. 4. The effectiveness of Loomis-Wood plots was greatly improved by this procedure and allowed to assign the vibrational satellite spectra of ν_{10} and ν_{22} despite the large discrepancy between the calculated and experimental values of their C rotational constants. While molecular parameters of the eight energetically lowest vibrationally excited states of cyclopentadiene are presented here, satellites from states even higher in energy were easily visible and could be assigned readily. However, a tentative analysis hinted towards strong interactions between multiple of these states, putting their quantitative analysis beyond the scope of this work.

⁴The CDMS results are used for the main isotopologue as they include more lines than Bogey et al. [4] and the III^1 representation is used.

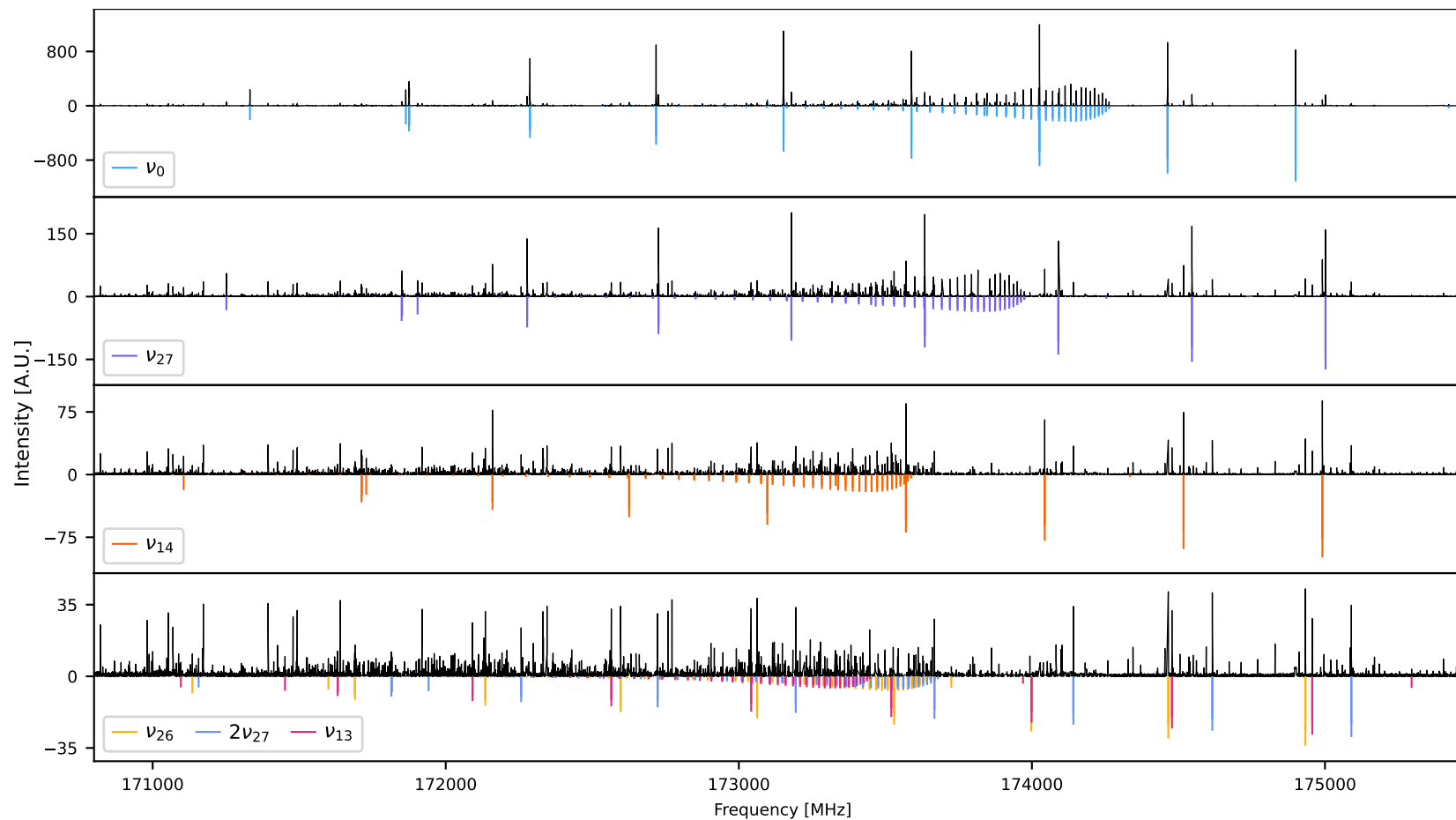


Figure 4: The process of removing known vibrationally excited states from the experimental spectrum visualized. In the top row, the complete spectrum is shown together with the predicted stick spectrum for the ground vibrational state in blue. Removing all data points within 2.5 MHz of the assigned ground state positions yields the spectrum in the row below (with the y -axis being rescaled to match the reduced data). There the predicted stick spectrum of the energetically lowest vibrationally excited state ν_{27} is shown in purple. Similarly, rows three and four show the spectrum after additionally removing lines belonging to ν_{27} and ν_{14} , respectively. This process greatly facilitates visual pattern recognition for vibrational states (and/or isotopologues) with lower intensities. The two lowest rows show that the method also has drawbacks, as some prominent lines from the predictions are missing in the experimental spectrum. This results from these lines being blended with transitions from already removed states. Combining this approach with Loomis-Wood plots increases the fault tolerance drastically.

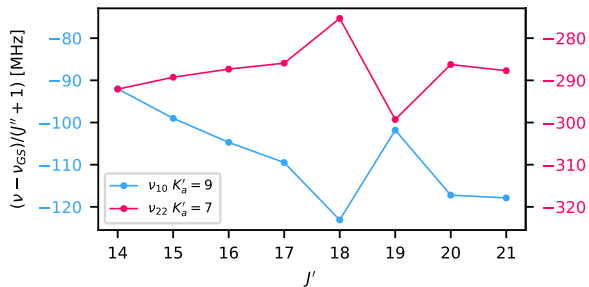


Figure 5: Resonance plot of the $K'_a = 9$ series of ν_{10} and the $K'_a = 7$ series of ν_{22} . In all transitions $\Delta J = \Delta K_a = \Delta K_c = 1$. The mirror image-like deviations for $J' = 18$ and 19 indicate an interaction that is centered around the respective energy levels with $J' = 18$.

Within the eight energetically lowest vibrational states analyzed here, two interaction systems could be identified by mirror images in their residuals and resonance plots (see Fig. 5), the ν_{10}/ν_{22} dyad and the $\nu_{26}/2\nu_{27}/\nu_{13}$ triad. The initial guess for the vibrational energy difference was approximated from the involved rotational energy levels. For the final model, 50 interstate transitions between ν_{13} and $2\nu_{27}$ as well as 20 interstate transitions between ν_{10} and ν_{22} were assigned. They result from wavefunction mixing due to the interactions and help determine the vibrational energy difference accurately. The interaction parameters were systematically tested with Pyckett⁵. From group theory it can be derived, that Coriolis interactions occur only between vibrational states of different symmetry and for each pair of states only a single symmetry (meaning a -, b -, or c - symmetry) of Coriolis interactions can occur [23–25].

The resulting rotational parameters of the vibrational states are given in Tab. 2 and the interaction parameters are given in Tab. 3. In general, the deviations of the rotational constants with respect to the ground vibrational state show good agreement with the rotation-vibration interaction constants from quantum chemical calculations, see Tab. A.1. Typically the obs-calc agreement is within 1 MHz but there are some slight deviations of about 2.5 MHz for α^A of ν_{10} and strong deviations for α^C of ν_{10} and ν_{22} of about ± 100 MHz. However, the $\alpha^C_{\nu_{10}} + \alpha^C_{\nu_{22}}$ values between the experiment and calculations agree well

⁵Pyckett is a Python wrapper around Pickett’s SPFIT and SPCAT [12]. It can be installed via `pip install pyckett`

(15.765(71) MHz and 15.01 MHz, respectively) [20, 27]. As mentioned, these systematic mirror image deviations result from Coriolis coupling contributions to the rotation-vibration interaction constant. Using equation 13 from Reference [20] and the values obtained from the quantum chemical calculations, the Coriolis interaction term of the rotation-vibration interaction constants is calculated to be about ± 103.42 MHz. By subtracting this term, the corrected calculated values, $\alpha^C_{\nu_{10},\text{corr}} = -111.18 \text{ MHz} + 103.42 \text{ MHz} = -7.76 \text{ MHz}$ and $\alpha^C_{\nu_{22},\text{corr}} = 96.17 \text{ MHz} - 103.42 \text{ MHz} = -7.25 \text{ MHz}$, agree with the experimental values within 1 MHz.

The two vibrational states closest in energy are the dyad as ν_{22} is only 5.1 cm^{-1} higher in energy than ν_{10} . The strongest interactions are observed for even ΔK_a values (see Fig. C.1) and the interstate transitions have even ΔK_a and odd ΔK_c values. For the triad, $2\nu_{27}$ lies in the middle, 7.9 cm^{-1} higher in energy than ν_{26} and 36.6 cm^{-1} lower than ν_{13} with the interactions between $2\nu_{27}$ and ν_{13} being the strongest and appearing for odd ΔK_a values (see Fig. C.2). The respective interstate transitions have even ΔK_a and ΔK_c values. The observed trends are similar for both interaction systems, with the center of the interaction increasing in K_a for increasing J . For the dyad, this pattern starts around $J'' = 14$ and $K''_a = 3/5$ whereas for ν_{13} and $2\nu_{27}$ the pattern starts around $J'' = 31$ and $K''_a = 0/1$.

For the interaction between ν_{10} and ν_{22} , only the relative signs of the interaction parameters can be determined (inverting the signs of all interaction parameters results in the same fit/predictions). For the triad, $\nu_{26}/2\nu_{27}/\nu_{13}$, there are four equivalent sets of interaction parameter signs (see Appendix F). Additionally, due to high correlations between the interaction parameters, the presented parameter set should be seen as one of many possible solutions.

The Coriolis G_α parameters between two fundamentals r and s were estimated from the results of the quantum chemical calculations as follows

$$G_\alpha(r, s) = \zeta_{r,s}^\alpha * B_e^\alpha * \left(\sqrt{\frac{\omega_r}{\omega_s}} + \sqrt{\frac{\omega_s}{\omega_r}} \right) \quad (1)$$

Here, $G_\alpha(r, s)$ are the Coriolis parameters of $\alpha = a, b, \text{ or } c$ symmetry, B_e^α the respective equilibrium rotational constant, ω the harmonic vibrations, and $\zeta_{r,s}^\alpha$ the respective Coriolis coefficients. As an approximation, we used the experimental ground vibrational state rotational constants for the B_e^α

Table 2: The resulting rotational parameters for the eight energetically lowest vibrationally excited states. The two interaction systems are indicated by blue and red colored table headers similar to Fig. 1.

Parameter	ν_{27}	ν_{14}	ν_{26}	$2\nu_{27}$	ν_{13}	$\nu_{27} + \nu_{14}$	ν_{10}	ν_{22}
A	/MHz 8429.339 717(69)	8418.480 575(89)	8408.255 59(13)	8431.9322(70)	8395.700 79(81)	8421.515(51)	8416.784(17)	8444.228(20)
B	/MHz 8214.788 334(61)	8207.517 052(80)	8217.218 58(15)	8204.4205(78)	8220.5890(49)	8197.100(49)	8227.977(17)	8227.153(19)
C	/MHz 4274.157 884(47)	4274.115 571(50)	4272.629 500(60)	4276.535 426(89)	4273.326 526(90)	4276.659 64(11)	4263.061(50)	4264.049(50)
$-D_J$	/kHz -2.696 942(27)	-2.682 148(34)	-2.646 176(95)	-2.706 45(22)	-2.583 22(32)	-2.684 18(41)	-2.6101(83)	-2.9493(84)
$-D_{JK}$	/kHz 4.062 326(43)	4.019 933(63)	3.944 34(31)	4.069 99(22)	3.728 32(65)	4.022 11(92)	4.951(12)	3.6197(86)
$-D_K$	/kHz -1.682 418(30)	-1.655 183(41)	-1.614 83(26)	a	-1.461 81(34)	-1.658 97(51)	-2.626(18)	-1.015(15)
d_1	/Hz -34.402(29)	-38.531(38)	-58.791(54)	a	-98.7(17)	a	a	a
d_2	/mHz 40(13)	a	a	a	a	a	a	a
Transitions	2117	1736	1146	441	437	572	572	550
Lines	1223	996	618	224	231	286	288	277
RMS	/kHz 22.07	22.47	26.90 ^b	26.90 ^b	26.90 ^b	21.79	25.06 ^c	25.06 ^c
$WRMS$	0.85	0.74	0.86 ^b	0.86 ^b	0.86 ^b	0.60	0.74 ^c	0.74 ^c

Fits performed with SPFIT in the S-reduction and III¹ representation. Standard errors are given in parentheses. Parameters of the ground vibrational state are applied to all vibrationally excited states and difference values are fitted. Parameters not specified were fixed to the global values, see Tab. 1. Interstate transitions are counted towards the lower state for the transitions and lines statistics. ^a Parameter was fixed to the global value. ^{b,c} Reported values are values for the respective combined fits.

Table 3: The resulting energy differences (colored analog to Fig. 1 and Tab. 1) and interaction parameters for the interactions between ν_{10} and ν_{22} as well as ν_{26} , $2\nu_{27}$, and ν_{13} .

v_1	v_2	ID ^a	Parameter	Value
			$\tilde{\nu}_{13} - \tilde{\nu}_{2 \times 27}$	/cm ⁻¹ 8.719 589(3)
$2\nu_{27}$	ν_{13}	$4000\nu_1\nu_2$	G_b	/MHz 407.6(15)
$2\nu_{27}$	ν_{13}	$4200\nu_1\nu_2$	G_{2b}	/kHz -8.720(99)
$2\nu_{27}$	ν_{13}	$4100\nu_1\nu_2$	F_{ac}	/MHz 3.166(25)
$2\nu_{27}$	ν_{13}	$4101\nu_1\nu_2$	$F_{ac,J}$	/Hz -120.35(40)
			$\tilde{\nu}_{13} - \tilde{\nu}_{26}$	/cm ⁻¹ 36.5867(2)
ν_{26}	ν_{13}	$6100\nu_1\nu_2$	F_{ab}	/MHz 6.4435(98)
			$\tilde{\nu}_{2 \times 27} - \tilde{\nu}_{26}$	/cm ⁻¹ 27.8671(2)
ν_{26}	$2\nu_{27}$	$2100\nu_1\nu_2$	F_{bc}	/MHz 2.521(16)
			$\tilde{\nu}_{22} - \tilde{\nu}_{10}$	/cm ⁻¹ 5.127 415(4)
ν_{10}	ν_{22}	$6000\nu_1\nu_2$	G_c	/MHz 4080.87(94)
ν_{10}	ν_{22}	$6200\nu_1\nu_2$	G_{2c}	/kHz -136.5(73)
ν_{10}	ν_{22}	$6210\nu_1\nu_2$	$G_{2c,K}$	/Hz 2.88(19)
ν_{10}	ν_{22}	$6100\nu_1\nu_2$	F_{ab}	/MHz 7.35(17)
ν_{10}	ν_{22}	$6110\nu_1\nu_2$	$F_{ab,K}$	/kHz 1.424(52)
ν_{10}	ν_{22}	$6101\nu_1\nu_2$	$F_{ab,J}$	/Hz 241(15)

^a The specified IDs are the respective parameter IDs used in the *.par and *.var files of SPFIT and SPCAT [12, 26].

values (see Tab. 1) and the harmonic wavenumbers from the quantum chemical calculations (see Tab. A.1) for the ω . For the dyad, this yields $G_c(\nu_{22}, \nu_{10}) = 7854$ MHz which is of same magnitude as the experimental value of 4080.85(14) MHz. For the triad, only the interaction between the two fundamentals ν_{13} and ν_{26} was estimated to be $G_c(\nu_{13}, \nu_{26}) = 875$ MHz. However, including $G_c(\nu_{13}, \nu_{26})$ did not improve the fit which hints toward the interaction parameters (especially for the triad) being effective.

The resulting weighted root mean square ($WRMS$) values are around 0.8 indicating that our uncertainties are slightly conservative. The analyses of the singly ¹³C substituted isotopologues have

significantly lower root mean square (RMS) and $WRMS$ values, which probably results from the lower number of assigned transitions and the limited frequency range (assignments were limited to frequencies below 250 GHz).

4. Structure determination

Using the improved rotational constants obtained in this work and refitting the line positions of the deuterium substituted isotopologues (1- d_1 , 1- d_2 , 1- d_3 , 1,2,3,4,5- d_5 , and d_6) from Damiani et al. [5], a semi-experimental equilibrium structure (r_e^{SE}) has been derived. Refitting the deuterium isotopic data was essential due to a typo in the A constant of cyclopentadiene 1,2,3,4,5- d_5 in Damiani et al. (7707.857(5) MHz [5] vs. 7007.857(11) MHz obtained here). For the deuterated isotopologues, the A_0 , B_0 , and C_0 rotational parameters were floated while the quartic centrifugal distortion parameters were fixed to their calculated values (fc-CCSD(T)/ANO0 level). All experimental isotopic A_0 , B_0 , and C_0 rotational constants were then corrected for the effects of zero-point vibration calculated at the fc-CCSD(T)/ANO0 level (see Tab. D.4) and the r_e^{SE} structure was derived with the STRFIT software [28]. A comparison of the r_e^{SE} structure against *ab initio* values calculated at the fc-CCSD(T)/ANO0 and ae-CCSD(T)/cc-pwCVQZ levels is given in Appendix D. As can be seen, the agreement between the r_e^{SE} and the high-level ae-CCSD(T)/cc-pwCVQZ structural parameters is excellent, to (well) within 10^{-3} Å and 0.1° for bond lengths and angles, respectively.

5. Conclusions

In the present study, the rotational spectrum coverage of cyclopentadiene was extended up to 510 GHz by measuring 250 GHz of high-resolution broadband spectra. This allowed to significantly increase the number of assigned lines for the main isotopologue from about 150 to 3510. As a result, the newly determined parameters produce much more reliable frequency predictions, especially for high frequencies and high quantum numbers (see Fig. E.3). Especially *R*-branch transitions above 330 GHz and *Q*-branch transitions are now in much better agreement. The presented data allows for astronomical searches at higher frequencies and over a much broader quantum number range. Similarly, the number of assigned lines for the three singly ^{13}C substituted isotopologues was increased from about 10 each to well over 200 each. Their frequency coverage was much improved from only microwave data to up to 250 GHz.

Lastly, the dominant vibrational satellite spectra of cyclopentadiene were described for the first time, including their interactions. Especially the energetically lowest-lying vibrational states are analyzed over a broad quantum number range permitting reliable predictions.

Future work might be targeted at deuterated isotopologues or vibrationally excited states higher in energy. Whereas analyses of deuterated isotopologues would be simplified by the use of enriched samples, the energetically higher vibrationally excited states could benefit from double-resonance techniques [29]. Additionally, the analyzed vibrational satellite spectrum is a great aid for rovibrational studies in the infrared. Rovibrational transitions between already analyzed states will be accurately predicted except for the band center and even rovibrational transitions with only one known vibrational state will benefit from the possibility of using techniques like the Automated Spectral Assignment Procedure [30].

Data availability

The input and output files of SPFIT will be provided as supplementary material.

Acknowledgments

We wish to acknowledge an anonymous referee for their careful reading of the manuscript and

providing useful suggestions. The authors from Cologne gratefully acknowledge the Collaborative Research Center 1601 (SFB 1601 sub-project A4) funded by the Deutsche Forschungsgemeinschaft (DFG, German Research Foundation) – 500700252.

J.-C.G. thanks the national program CNRS PCMI (Physics and Chemistry of the Interstellar Medium) and the CNES for a grant (CMISTEP).

Appendix A. Vibrational wavenumbers and rotation-vibration interaction constants

Table A.1: Rotation-vibration interaction constants α_i , harmonic and anharmonic wavenumbers $\tilde{\nu}_i$ from quantum chemical calculations at the CCSD(T)/ANO0 level as well as the wavenumbers reported by Castellucci et al. [7]. Rotation-vibration interaction constants are in MHz and wavenumbers in cm^{-1} . Literature values are taken from liquid phase spectra if not specified otherwise.

Mode		$-\alpha_{\text{calc}}^A$	$-\alpha_{\text{calc}}^B$	$-\alpha_{\text{calc}}^C$	$\tilde{\nu}_{\text{calc}}^{\text{anh}}$	$\tilde{\nu}_{\text{calc}}^{\text{harm}}$	$\tilde{\nu}_{\text{lit}}$ [7]
ν_{27}	B_1	3.77	-11.22	2.93	339	340	350
ν_{14}	A_2	-6.86	-17.19	2.74	497	502	516 ^a
ν_{26}	B_1	-16.56	-8.26	1.15	658	670	664 ^b
ν_{13}	A_2	-30.06	-4.22	1.94	691	701	700
ν_{10}	A_1	-6.44	2.62	-111.18	789	799	802
ν_{22}	B_2	18.45	2.51	96.17	793	804	805
ν_{25}	B_1	-830.70	-33.86	-0.80	896	920	891
ν_{12}	A_2	-19.44	-55.71	-0.81	897	917	941 ^a
ν_9	A_1	815.34	27.89	-20.22	903	920	915
ν_{24}	B_1	2.38	-12.17	0.22	905	927	925
ν_{21}	B_2	-11.03	23.84	5.81	953	972	959
ν_8	A_1	2.39	-14.20	-4.82	1015	1006	994
ν_{20}	B_2	17.40	7.20	-4.29	1085	1104	1090
ν_7	A_1	14.67	-1.33	2.07	1102	1120	1106
ν_{11}	A_2	-8.06	-0.53	2.43	1102	1131	1100 ^a
ν_{19}	B_2	-0.34	1.60	-9.04	1236	1266	1239
ν_{18}	B_2	-1.90	0.52	-8.39	1278	1310	1292
ν_6	A_1	2.59	-3.70	-5.98	1360	1393	1365
ν_5	A_1	-4.14	9.97	7.68	1389	1428	1378
ν_4	A_1	-17.62	-4.69	-5.98	1503	1547	1500
ν_{17}	B_2	-15.81	-3.48	-4.02	1572	1615	1580
ν_3	A_1	-4.70	-4.77	-0.72	2905	3042	2886
ν_{23}	B_1	-3.34	-3.42	-1.21	2929	3086	2900
ν_{16}	B_2	-6.12	-7.20	-3.40	3084	3216	3043
ν_2	A_1	-6.23	-7.71	-3.53	3090	3225	3075
ν_1	A_1	-6.84	-7.91	-3.67	3113	3250	3091
ν_{15}	B_2	-6.86	-7.52	-3.53	3115	3242	3105

^a Solid-phase value (other literature energy values are taken from liquid phase spectra).

^b Gas-phase high-resolution infrared spectroscopy yields a value of 663.84800(5) cm^{-1} [6].

Appendix B. Rotational constants from literature and quantum chemical calculations

Table B.2: Literature values of the rotational constants for the main isotopologue (from the CDMS [31, 32]) and for the singly substituted ^{13}C isotopologues (from Damiani et al. [5])

Param.		<i>c</i> -C ₅ H ₆ [31, 32]	1- ¹³ C [5]	2- ¹³ C [5]	3- ¹³ C [5]
<i>A</i>	/MHz	8426.1111(11)	8226.028(9)	8419.949(6)	8345.097(10)
<i>B</i>	/MHz	8225.6387(11)	8219.434(7)	8040.358(6)	8108.662(7)
<i>C</i>	/MHz	4271.4377(11)	4217.760(6)	4219.419(4)	4219.067(7)
$-D_J$	/kHz	-2.6948(13)	-	-	-
$-D_{JK}$	/kHz	4.0626(29)	-	-	-
$-D_K$	/kHz	-1.6842(17)	-	-	-
<i>d</i> ₁	/Hz	-39.7(18)	-	-	-
Transitions		157	-	-	-
Lines		92	-	-	-
<i>RMS</i>	/kHz	30.68	-	-	-
<i>WRMS</i>		1.02	-	-	-

Table B.3: Quartic centrifugal distortion constants (III¹ representation) of the main isotopologue and the singly substituted ^{13}C isotopologues as calculated at the fc-CCSD(T)/ANO0 level.

Param.		<i>c</i> -C ₅ H ₆	1- ¹³ C	2- ¹³ C	3- ¹³ C
$-D_J$	/kHz	-2.587 44	-2.546 47	-2.529 34	-2.5328
$-D_{JK}$	/kHz	3.895 13	3.836 87	3.809 24	3.817 31
$-D_K$	/kHz	-1.611 71	-1.588 84	-1.577 39	-1.581 23
<i>d</i> ₁	/Hz	-44.0093	61.0209	-20.1082	-11.8137
<i>d</i> ₂	/Hz	0.751 250	-2.719 14	-3.629 88	1.226 95

Appendix C. Interaction hotspots

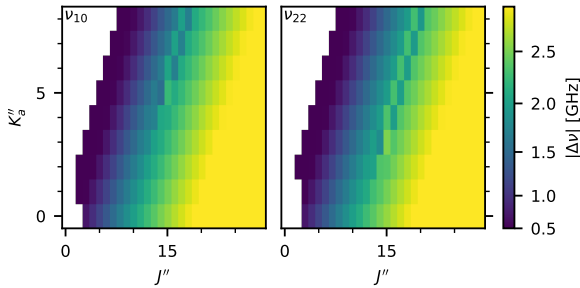


Figure C.1: Absolute shifts in transition frequency between predictions with and without interactions for $\Delta J_{\Delta K_a, \Delta K_c} = 1_{1,1}$ transitions. The heatmaps of the interacting vibrational states ν_{10} (left) and ν_{22} (right) show the same pattern when shifted by $\Delta K_a = 2$. The center of the interactions increases in K_a with increasing J value.

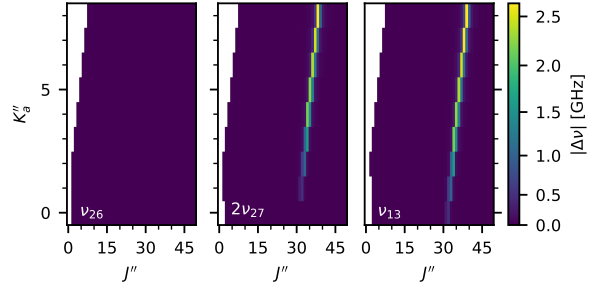


Figure C.2: Absolute shifts in transition frequency between predictions with and without interactions for $\Delta J_{\Delta K_a, \Delta K_c} = 1_{1,1}$ transitions. The heatmaps of the interacting vibrational states ν_{26} (left), $2\nu_{27}$ (middle) and ν_{13} (right) highlight that the strongest interactions are between $2\nu_{27}$ and ν_{13} with $\Delta K_a = 2$. The center of the interactions increases in K_a with increasing J value. In contrast to Fig. C.1, the x -axis and the z -axis (being the heatmap color) are scaled differently to highlight the main interactions better.

Appendix D. Semi-experimental equilibrium structure

Table D.4: Rotational constants (MHz) and zero-point vibrational corrections (fc-CCSD(T)/ANO0, MHz) of cyclopentadiene isotopologues.

	<i>c</i> -C ₅ H ₆	1- ¹³ C ₁	2- ¹³ C	3- ¹³ C	1- <i>d</i> ₁	1- <i>d</i> ₂	1- <i>d</i> ₃	1,2,3,4,5- <i>d</i> ₅	<i>d</i> ₆
<i>A</i> ₀	8426.109	8226.053	8420.043	8345.132	8129.952	8414.045	8307.036	7007.858	6608.398
<i>B</i> ₀	8225.640	8219.483	8040.425	8108.714	7859.534	7591.889	7678.126	6681.888	6007.340
<i>C</i> ₀	4271.437	4217.759	4219.411	4219.065	4145.090	4091.154	4090.254	3529.302	3444.129
ΔA	63.046	66.046	62.748	63.249	65.660	63.130	64.793	49.690	48.552
ΔB	66.461	60.796	64.627	63.844	58.864	58.628	56.982	48.475	46.425
ΔC	34.228	33.512	33.672	33.580	33.263	32.018	31.969	25.954	25.158
<i>A</i> ₀ ^{SE}	8489.155	8292.100	8482.792	8408.381	8195.612	8477.175	8371.829	7057.549	6656.950
<i>B</i> ₀ ^{SE}	8292.102	8280.279	8105.053	8172.558	7918.399	7650.517	7735.108	6730.363	6653.765
<i>C</i> ₀ ^{SE}	4305.665	4251.271	4253.082	4252.645	4178.353	4123.172	4122.222	3555.255	3469.288

Equilibrium structural parameters of cyclopentadiene (bond lengths in Å, angles in degrees) calculated at the fc-CCSD(T)/ANO0 and ae-CCSD(T)/cc-pwCVQZ levels of theory and determined semi-experimentally. See text for details.

```
X
X 1 rd
C 2 rd 1 a90
C 3 r1 2 a1 1 d90
C 3 r1 2 a1 4 d180
C 4 r2 3 a2 5 d0
C 5 r2 3 a2 4 d0
H 4 r3 3 a3 2 d180
H 5 r3 3 a3 2 d180
H 6 r4 4 a4 8 d0
H 7 r4 5 a4 9 d0
H 3 r5 2 a5 1 d0
H 3 r5 2 a5 12 d180
```

```
rd = ANOO / pwCVQZ / reSE
      1.0 / 1.0 / 1.0
```

a90	=	90.0	/	90.0	/	90.0
r1	=	1.515110	/	1.500253	/	1.49906(34)
a1	=	51.526426	/	51.537508	/	51.541(15)
d90	=	90.0	/	90.0	/	90.0
d180	=	180.0	/	180.0	/	180.0
r2	=	1.361296	/	1.346357	/	1.34635(35)
a2	=	109.368447	/	109.329183	/	109.330(24)
d0	=	0.0	/	0.0	/	0.0
r3	=	1.087290	/	1.078491	/	1.07865(24)
a3	=	124.008184	/	124.075312	/	124.01(11)
r4	=	1.087975	/	1.079202	/	1.07907(22)
a4	=	126.235302	/	126.127498	/	126.082(60)
r5	=	1.102197	/	1.093823	/	1.09441(17)
a5	=	126.576616	/	126.701234	/	126.710(12)

Appendix E. Comparison of initial and final residuals

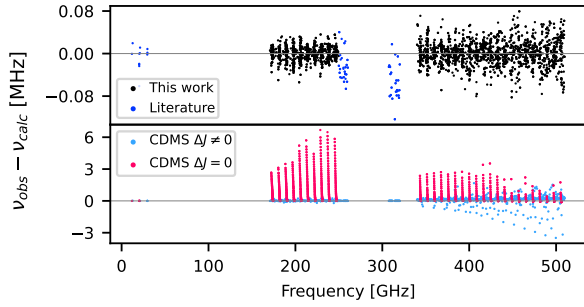


Figure E.3: Residuals of the ground vibrational state of the main isotopologue for the predictions from this work (top) compared with the residuals for the predictions from the CDMS [31, 32] (based on data of previous reports [1, 4]). Colors distinguish between literature assignments and new assignments in the top row and between Q - and R -branch transitions in the bottom row. This work greatly improves predictions for R -branch transitions above 330 GHz and Q -branch transitions above 40 GHz.

Appendix F. Signs of Coriolis interaction parameters

It is common when treating Coriolis interactions that there are multiple equivalent parameter sets for the analysis which only differ in the signs of the Coriolis interaction parameters [33, 34]. Even though the calculated Coriolis interaction parameters have a defined sign, it typically cannot be determined experimentally. The equivalent interaction parameter sets of the ν_{10}/ν_{22} diad are

$$\begin{aligned} & \{G_c, G_{2c}, G_{2c,K}, F_{ab}, F_{ab,K}, F_{ab,J}\} \\ & \{-G_c, -G_{2c}, -G_{2c,K}, -F_{ab}, -F_{ab,K}, -F_{ab,J}\} \end{aligned} \quad (\text{F.1})$$

This means inverting all parameter signs results in exactly the same fit/frequency predictions. The triad, being ν_{26} , $2\nu_{27}$, and ν_{13} , has four equivalent interaction parameter sets, being

$$\begin{aligned} & \{G_b^{12}, G_{2b}^{12}, F_{ac}^{12}, F_{ac,J}^{12}, F_{bc}^{01}, F_{ab}^{02}\} \\ & \{G_b^{12}, G_{2b}^{12}, F_{ac}^{12}, F_{ac,J}^{12}, -F_{bc}^{01}, -F_{ab}^{02}\} \\ & \{-G_b^{12}, -G_{2b}^{12}, -F_{ac}^{12}, -F_{ac,J}^{12}, -F_{bc}^{01}, -F_{ab}^{02}\} \\ & \{-G_b^{12}, -G_{2b}^{12}, -F_{ac}^{12}, -F_{ac,J}^{12}, F_{bc}^{01}, F_{ab}^{02}\} \end{aligned} \quad (\text{F.2})$$

where for brevity the superscript indices specifying the vibrational states are given as their respective vibrational identifiers used in the `*.par` file of SP-FIT: $0 \equiv \nu_{26}$, $1 \equiv \nu_{13}$, and $2 \equiv 2\nu_{27}$.

For both interacting systems, the relative signs within one Coriolis symmetry and two-state connection have to stay fixed. For the triad, the signs for the different Coriolis symmetries can be exchanged in pairs.

References

- [1] L. H. Scharpen, V. W. Laurie, Structure of Cyclopentadiene, *J. Chem. Phys.* 43 (1965) 2765–2766. doi:10.1063/1.1697207.
- [2] V. W. Laurie, Microwave Spectrum and Dipole Moment of Cyclopentadiene, *J. Chem. Phys.* 24 (1956) 635–636. doi:10.1063/1.1742585.
- [3] R. C. Benson, W. H. Flygare, Molecular Zeeman Effect of Cyclopentadiene and Isoprene and Comparison of the Magnetic Susceptibility Anisotropies, *J. Am. Chem. Soc.* 92 (1970) 7523–7529. doi:10.1021/ja00729a001.
- [4] M. Bogey, C. Demuyneck, J. L. Destombes, The millimeter wave spectrum of cyclopentadiene, *J. Mol. Spectrosc.* 132 (1988) 277–279. doi:10.1016/0022-2852(88)90074-4.
- [5] D. Damiani, L. Ferretti, E. Gallinella, Structure of cyclopentadiene from microwave spectra of several deuterated species, *Chem. Phys. Lett.* 37 (1976) 265–269. doi:10.1016/0009-2614(76)80212-6.
- [6] S. R. Boardman, S. A. Bone, P. B. Davies, N. A. Martin, High-resolution FTIR and diode laser jet spectroscopy of cyclopentadiene, *J. Mol. Spectrosc.* 143 (1990) 100–110. doi:10.1016/0022-2852(90)90264-q.
- [7] E. Castellucci, P. Manzelli, B. Fortunato, E. Gallinella, P. Mirone, Vibrational spectra and normal-coordinate treatment of cyclopentadiene and its deuterated derivatives, *Spectrochim. Acta A* 31 (1975) 451–461. doi:10.1016/0584-8539(75)80037-7.
- [8] J. Cernicharo, M. Agúndez, C. Cabezas, B. Tercero, N. Marcelino, J. R. Pardo, P. de Vicente, Pure hydrocarbon cycles in TMC-1: Discovery of ethynyl cyclopropenylidene, cyclopentadiene, and indene, *Astron. Astrophys.* 649 (2021) L15. doi:10.1051/0004-6361/202141156.
- [9] M. A. Martin-Drumel, J. van Wijngaarden, O. Zingsheim, F. Lewen, M. E. Harding, S. Schlemmer, S. Thorwirth, Millimeter- and submillimeter-wave spectroscopy of disulfur dioxide, *OSSO, J. Mol. Spectrosc.* 307 (2015) 33–39. doi:10.1016/j.jms.2014.11.007.

- [10] B. Helmstaedter, Sub-millimeter Rotational Spectroscopy of Cyclopentadiene – An Analysis of the Ground State and Vibrational Satellite Spectrum up to 250 GHz, Master’s thesis, I. Physikalisches Institut, Universität zu Köln (2024).
- [11] L. Bonah, O. Zingsheim, H. S. P. Müller, J.-C. Guillemin, F. Lewen, S. Schlemmer, LLWP—A new Loomis-Wood software at the example of Acetone- $^{13}\text{C}_1$, *J. Mol. Spectrosc.* 388 (2022) 111674. doi:10.1016/j.jms.2022.111674.
- [12] H. M. Pickett, The fitting and prediction of vibration-rotation spectra with spin interactions, *J. Mol. Spectrosc.* 148 (1991) 371–377. doi:10.1016/0022-2852(91)90393-o.
- [13] L. Bonah, S. Schlemmer, J.-C. Guillemin, M. E. Harding, S. Thorwirth, On the spectroscopy of phosphalkynes: Millimeter- and submillimeter wave study of $\text{C}_2\text{H}_5\text{CP}$, *J. Phys. Chem. A* 128 (2024) 4859–4866. doi:10.1021/acs.jpca.4c02566.
- [14] D. A. Matthews, L. Cheng, M. E. Harding, F. Lipparini, S. Stopkowicz, T.-C. Jagau, P. G. Szalay, J. Gauss, J. F. Stanton, Coupled-cluster techniques for computational chemistry: The CFOUR program package, *The Journal of Chemical Physics* 152 (2020). doi:10.1063/5.0004837.
- [15] M. E. Harding, T. Metzroth, J. Gauss, A. A. Auer, Parallel calculation of CCSD and CCSD(T) analytic first and second derivatives, *J. Chem. Theory Comput.* 4 (2008) 64–74. doi:10.1021/ct700152c.
- [16] C. Puzzarini, J. F. Stanton, J. Gauss, Quantum-chemical calculation of spectroscopic parameters for rotational spectroscopy, *Int. Rev. Phys. Chem.* 29 (2010) 273–367. doi:10.1080/01442351003643401.
- [17] K. Raghavachari, G. W. Trucks, J. A. Pople, M. Head-Gordon, A fifth-order perturbation comparison of electron correlation theories, *Chem. Phys. Lett.* 157 (1989) 479–483. doi:10.1016/s0009-2614(89)87395-6.
- [18] J. Almlöf, P. R. Taylor, General contraction of Gaussian basis sets. I. Atomic natural orbitals for first- and second-row atoms, *J. Chem. Phys.* 86 (1987) 4070–4077. doi:10.1063/1.451917.
- [19] S. Thorwirth, M. E. Harding, J. B. Dudek, M. C. McCarthy, Equilibrium molecular structures of vinyl carbon chains: Vinyl acetylene, vinyl diacetylene, and vinyl cyanide, *J. Mol. Spectrosc.* 350 (2018) 10–17. doi:10.1016/j.jms.2018.05.001.
- [20] I. M. Mills, *Vibration-rotation structure in asymmetric and symmetric top molecules*, Academic Press, 1972, pp. 115–140.
- [21] E. Tørneng, C. J. Nielsen, P. Klaeboe, H. Hopf, H. Priebe, The i.r., Raman and microwave spectra of 1-butene-3-yne (vinylacetylene) and 1-butene-3-yne-4d, *Spectrochim. Acta A* 36 (1980) 975–987. doi:10.1016/0584-8539(80)80177-2.
- [22] C. P. Endres, G. C. Mellau, M. E. Harding, M.-A. Martin-Drumel, H. Lichau, S. Thorwirth, High-resolution infrared study of vinyl acetylene: The ν_{13} (214 cm^{-1}) and ν_{18} (304 cm^{-1}) fundamentals, *J. Mol. Spectrosc.* 379 (2021) 111469. doi:10.1016/j.jms.2021.111469.
- [23] H. A. Jahn, Note on Coriolis Coupling Terms in Polyatomic Molecules, *Phys. Rev.* 56 (1939) 680–683. doi:10.1103/physrev.56.680.
- [24] D. R. J. Boyd, H. C. Longuet-Higgins, Coriolis interaction between vibration and rotation in symmetric top molecules, *Proc. R. Soc. Lond. Ser. A* 213 (1952) 55–73. doi:10.1098/rspa.1952.0110.
- [25] I. M. Mills, Coriolis interactions, intensity perturbations and potential functions in polyatomic molecules, *Pure Appl. Chem.* 11 (1965) 325–344. doi:10.1351/pac196511030325.
- [26] B. J. Drouin, Practical uses of SPFIT, *J. Mol. Spectrosc.* 340 (2017) 1–15. doi:10.1016/j.jms.2017.07.009.
- [27] J. M. L. Martin, J. P. Francois, R. Gijbels, The Anharmonic Force Field of Thioformaldehyde, H_2CS , by ab Initio Methods, *J. Mol. Spectrosc.* 168 (1994) 363–373. doi:10.1006/jmsp.1994.1285.
- [28] Z. Kisiel, Least-squares mass-dependence molecular structures for selected weakly bound intermolecular clusters, *J. Mol. Spectrosc.* 218 (2003) 58–67. doi:10.1016/s0022-2852(02)00036-x.
- [29] O. Zingsheim, L. Bonah, F. Lewen, S. Thorwirth, H. S. P. Müller, S. Schlemmer, Millimeter-millimeter-wave double-modulation double-resonance spectroscopy, *J. Mol. Spectrosc.* 381 (2021) 111519. doi:10.1016/j.jms.2021.111519.
- [30] M. A. Martin-Drumel, C. P. Endres, O. Zingsheim, T. Salomon, J. van Wijngaarden, O. Pirali, S. Gruet, F. Lewen, S. Schlemmer, M. C. McCarthy, S. Thorwirth, The SOLEIL view on sulfur rich oxides: The S_2O bending mode ν_2 at 380 cm^{-1} and its analysis using an Automated Spectral Assignment Procedure (ASAP), *J. Mol. Spectrosc.* 315 (2015) 72–79. doi:10.1016/j.jms.2015.02.014.
- [31] C. P. Endres, S. Schlemmer, P. Schilke, J. Stutzki, H. S. P. Müller, The Cologne Database for Molecular Spectroscopy, CDMS, in the Virtual Atomic and Molecular Data Centre, VAMDC, *J. Mol. Spectrosc.* 327 (2016) 95–104. doi:10.1016/j.jms.2016.03.005.
- [32] H. S. P. Müller, S. Thorwirth, D. A. Roth, G. Winnewisser, The Cologne Database for Molecular Spectroscopy, CDMS, *Astron. Astrophys.* 370 (2001) L49–L52. doi:10.1051/0004-6361:20010367.
- [33] K. Islami, B. P. Winnewisser, J. Preusser, M. Winnewisser, $\text{H}^{13}\text{C}^{14}\text{NO}$: Independent Parameters Describing the Coriolis Resonance Systems (00002)/(00010) and (00012)/(00020), *J. Mol. Spectrosc.* 176 (1996) 403–415. doi:10.1006/jmsp.1996.0102.
- [34] H. S. P. Müller, A. Maeda, F. Lewen, S. Schlemmer, I. R. Medvedev, E. Herbst, Rotational spectroscopy of the thioformaldehyde isotopologues H_2CS and $\text{H}_2\text{C}^{34}\text{S}$ in four interacting excited vibrational states and an account on the rotational spectrum of thioketene, H_2CCS , *Mol. Phys.* 122 (2023). doi:10.1080/00268976.2023.2262057.